Koltzer *et al. Geothermal Energy* (2023) 11:2
https://doi.org/10.1186/s40517-023-00245-7

Geothermal Energy

RESEARCH Open Access

How temperatures derived from fluid flow and heat transport models impact predictions of deep geothermal potentials: the "heat in place" method applied to Hesse (Germany)

Nora Koltzer[1,2,3*], Judith Bott[1], Kristian Bär[4] and Magdalena Scheck-Wenderoth[1,2]

*Correspondence:
koltzer@gfz-potsdam.de

[1] Basin Modelling, Helmholtz Centre Potsdam GFZ German Research Centre for Geosciences, Potsdam, Germany
[2] Faculty of Georesources and Material Engineering, RWTH Aachen, Aachen, Germany
[3] Fraunhofer Research Institution for Energy Infrastructures and Geothermal Systems IEG, Bochum, Germany
[4] GeoThermal Engineering GmbH, Karlsruhe, Germany

Abstract

One key aspect in the energy transition is to use the deep geothermal energy stored in sedimentary basins as well as in igneous and metamorphic basement rocks. To estimate the variability of deep geothermal potentials across different geological domains as encountered in the Federal State of Hesse (Germany), it is necessary to understand the driving processes of fluid flow and heat transport affecting subsurface temperature variations. In this study, we quantify the stored energy in a set of geological units in the subsurface of Hesse with the method of "heat in place" (HIP, sensu Muffler and Cataldi in Geothermics 7:53–89, 1978)—HIP is one proxy for the geothermal potential of these units controlled by their temperature configuration as derived from a series of coupled 3D thermo-hydraulic numerical models. We show how conductive, advective and convective heat transport mechanisms influence the thermal field and thereby the HIP calculations. The heterogeneous geology of the subsurface of Hesse ranges from locally outcropping Paleozoic basement rocks to up to 3.8 km thick Cenozoic, porous sedimentary deposits in the tectonically active northern Upper Rhine Graben. The HIP was quantified for five sedimentary layers (Cenozoic, Muschelkalk, Buntsandstein, Zechstein, Rotliegend) as well as for the underlying basement. We present a set of maps allowing to identify geothermally prospective subregions of Hesse based on the laterally varying thermal energy stored within the units. HIP is predicted to be highest in the area of the northern Upper Rhine Graben in the Cenozoic unit with up to 700 GJ m^{-2} and in the Rotliegend with up to 617 GJ m^{-2}. The calculations account for the variable thicknesses and temperatures of the layers, density and heat capacity of the solid and fluid parts of the rocks as well as porosity.

Keywords: Upper Rhine Graben, Hessen, Heat in place, 3D Hydrothermal Model, Geothermal energy, Geothermal potential, Heat transport

Introduction

For heating and cooling, in Germany 56% of the energy is used and only 15% are from renewable resources (Bracke et al. 2022). This reveals the importance of focusing geothermal energy production not only on power generation but consider its suitability for

heating and cooling purposes as well. Therefore, potential geothermal energy that can be derived from the subsurface can play an important role also in the context of the current energetic and heat transition discussed in Germany, while moving away from coal and nuclear to more environmentally friendly, renewable energy sources.

Most of the currently exploited deep geothermal energy worldwide comes from active high-enthalpy hydrothermal reservoirs (Trumpy et al. 2016; Kivanc Ates and Serpen 2016; Aravena et al. 2016; Wang et al. 2021). Investments in the exploration of low enthalpy hydrothermal systems however are largely hampered by the high risks related to discovering lower temperatures and/or less fluid producing conditions than anticipated (Sass et al. 2017). Detailed exploration of a potential site (through geophysical methods or exploration wells boreholes, for example) is very cost intensive (Bär et al. 2021). Before taking decisions on such a particular site, stakeholders would want to rely on regional estimations of the variability of geothermal potentials. This requires, however, profound knowledge of the subsurface geology and in particular its thermal and hydrogeological characteristics (Bär et al. 2011, 2020, 2021). When potential geothermal resources are predicted, most authors rely on purely conductive heat transport models either in 1D or 3D [e.g., (Calcagno et al. 2014; Bèdard et al. 2020)]. This is convincing, as temperature measurements can often be fitted with these models and the computation time is much less expensive in comparison to fully coupled 3D thermo-hydraulic simulations. The good prediction of deep temperature is one key aspect for the quality of the prediction of geothermal potential. Purely conductive simulations, however, are not convincing in regions, clearly influenced by fluid flow, like the Upper Rhine Graben area, or other sedimentary basins with deep porous aquifer layers. In such convection-dominated regions differences between measured subsurface temperatures and purely conductive models can exceed up to $\pm$ 50 °C. Therefore, we used thermo-hydraulic simulations to predict the deep temperature distribution, like in the recent work from Huang et al. (2022) to involve the physical complexity of heat transport into the prediction of the HIP. We have extensively studied the deep thermal and hydraulic field of the entire Federal State of Hesse (Germany) by means of 3D thermohydraulic simulations as based on regional geological models (Koltzer et al. 2019a). With the present study, we want to develop this approach further as we calculate the amounts of energy stored in the different geological units according to different temperature distributions as obtained by assuming different heat transport mechanisms being at play. More precisely, our approach combines a 3D geological structural model of Hesse (Arndt et al. 2011) with temperatures predicted by different thermohydraulic simulations (Koltzer et al. 2019a) to derive the "heat in place" (HIP, sensu Garg and Combs 2015; Muffler and Cataldi 1978) as one proxy for the range and distribution of the geothermal potential in the study area (Fig. 1). In this study, the focus lies on the application of new, complex and detailed numerical models for the fundamental assessment of geothermal potential with the HIP method. With this work it is possible to directly draw conclusions on the effects of the interplay of different heat transport processes (conduction, advection and convection) on the geothermal potential assessment.

There is no unique way to assess the geothermal potential related to a particular geothermal resource. Many studies in this field make use of the basic concept of the HIP method after Muffler and Cataldi (1978) to provide a volumetric quantification of the

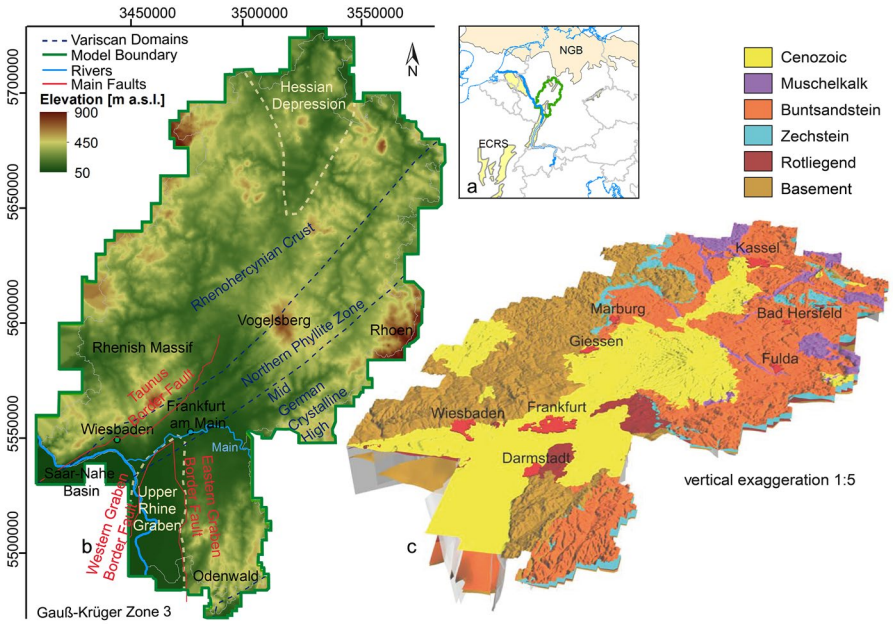

Fig. 1 **a** Position of the model area marked by a green contour; sediments of the European Cenozoic Rift System (ECRS) in yellow and of the North German Basin (NGB) in pale yellow; **b** topographic map of Hesse [modified after Koltzer et al. (2019a); topography: NOAA National Geophysical Data Center (2009)]. **c** Structural model of Hesse, the view is from southeast [modified after Arndt et al. (2011)]. The used graphics software was (Adobe Inc. 2019)

thermal energy of a reservoir (e.g. Lovekin 2004; Williams et al. 2008; van Wees et al. 2012; Zarrouk and Moon 2014; Garg and Combs 2015; Aravena et al. 2016; Limberger et al. 2018) With this method it is also possible to estimate geothermal potential in high-to-low prospective areas as classes (Magri et al. 2014; Bär 2012; Arndt et al. 2011). More detailed predictions including the performance of for example a hydrothermal doublet (van Wees et al. 2012; Kastner et al. 2015) need detailed assumptions about the type of utilization, the technical implementation and operating efficiency. As these parameters are strongly dependent on the location and are not yet worked out for each reservoir layer throughout the entire region of the Federal State of Hesse, we decided to apply the fundamental HIP method (Nathenson 1975; Muffler and Cataldi 1978; Garg and Combs 2015) which considers the natural subsurface conditions and profit from our highly complex physical thermal models. Predictions of the HIP, which is a theoretical potential is sufficient for a regional scoping of high and low prospective areas. The HIP calculated within this study could, therefore, be seen as the maximal theoretical potential and needs to be further limited with technical and ecological aspects and parameters as the injection temperature, the recovery factor and the power plant efficiency (e.g., Rogge and Kaltschmitt 2002; Paschen et al. 2003; Eyerer et al. 2020). After O'Sullivan and O'Sullivan (2016) the theoretical potential needs to by multiplied with a recovery factor. The recovery factor is not only site specific and dependent on the thermal conductivity, permeability and viscosity (Fan et al. 2022), it can also change with time (Gringarten 1978; Sanyal and Butler 2005; Williams 2007, 2010; Rybach 2010). The general trend of high and low prospective regions is dependent on the geology and the thermal field. Mostly the absolute value of extractable energy is sensitive to the applied method

to predict the geothermal potential. This was shown in Marrero-Diaz et al. (2015), where HIP and extractable heat are predicted to vary in absolute values, but the spatial distribution stays the same. This prediction of the most promising region in the URG, based on the thermal simulations of Koltzer et al. (2019a) is in agreement with conclusions derived from previous investigations about the geothermal potential. Antics and Sanner (2007) described the area of the URG as a high-temperature basinal system potentially providing enough heat for district heating and, possibly, for electric power generation (Antics and Sanner 2007). In addition, the URG has also been described as a potential subsurface resource for direct-use heating/cooling projects for temperatures below 150 °C (Lund 2018) or as a hot water aquifer for direct-use with temperatures between 60 and 100 °C (Schellschmidt et al. 2010). In addition, one of the main outcomes of the international Interreg IV Project GeORG was to conclude that the URG was characterized in general by promising geothermal potentials (GeORG-Projektteam 2013a, b, c, d). The main research question of this study is: what are the influences of conductive, advective and convective heat transport processes on the predicted geothermal potentials (HIP) across Hesse?

Heat in place method to calculate geothermal potential for Hesse

With the HIP method (Muffler and Cataldi 1978), it is possible to quantify the heat (H) stored in a given volume (V) in the subsurface as formulated in Eq. 1:

$$H = V\left((1-\varphi)\rho_{\mathrm{m}}c_{\mathrm{p,m},T_{\mathrm{r}}} + \varphi\rho_{\mathrm{f}}c_{\mathrm{p,f}}\right)\cdot(T_{\mathrm{r}} - T_{\mathrm{ref}}) \tag{1}$$

As properties density (ρ) and heat capacity (c_{p}) for each unit are considered for the rock matrix (m) and for the pore fluid (f), weighted to a sum by the porosity (φ). The density and heat capacity of the solid rock phase and the density of the fluid are considered to be lithology dependent (Table 1). The content of volumetric heat corresponds to the temperature (T) difference between the reservoir (r) and a reference (ref) temperature. Details on the parametrization are provided in the following sections.

Based on the 3D geological model and the respective thermal models ("Thermal models of Hesse" section), we are able to quantify the volumetric heat of a particular geological unit piecewise according to the horizontal grid spacing. Hence, for each grid point location (X, Y), the volume (V) of a geological unit is calculated by multiplying the thickness of the unit with 1 m^2, which finally results in mapped distributions of calculated HIP per square meter (J m^{-2}). We take the modelled temperature at the exact vertical middle of a unit as a representative average reservoir temperature (T_{r}). The depth distribution (Fig. 2) is derived based on the topologies of the units' top and base interfaces (Eq. 2). We solved all relevant equations (Eqs. 1, 3, 4, 5, 6, 7) with a python tool, which will be available as Bott et al. (2022).

Input data for HIP calculations

The calculation of the HIP relies on a huge database expressed in different temperature predictions. These predictions are results from a former study on hydraulic, thermal and coupled hydrothermal heat transport processes in the study area (Koltzer et al. 2019a). To simulate the thermohydraulic behavior of the system, a very detailed 3D structural model Arndt (2012) (Fig. 1c) was used, which in this study is used to predict the HIP as

Table 1 Parameters used for each geological unit (C: Cenozoic, M: Muschelkalk, BS: Buntsandstein, Z: Zechstein, R: Rotliegend, B: Basement) to calculate the HIP

Unit	Rock						Fluid					
	Effective porosity		Density		Specific heat capacity		Specific heat capacity		Salinity		Density	
	φ [–]	Ref.	ρ_m [kg m^{-3}]	Ref.	$c_{p,m,T_{20}}$ [J/(kg*K)-1]	Ref.	$c_{p,f}$ [J/(kg*K)-1]	Ref.	S [g l^{-1}]	Ref.	$\rho_{f,T_{20}}$ [kg m^{-3}]	Ref.
C	0.14	1	2680	1	810	1	3925	1	60	1	1040	7
M	0.04	3	2502	9	675	8	3925	1	75	5	1060	7
BS	0.14	2	2650	2	705	3	3925	1	100	5	1070	7
Z	0.12	3	2365	9	796	8	3925	1	110	10	1080	7
R	0.09	3	2730	4	758	3	3925	1	130	6	1120	7
B	0.04	1	2719	1	695	1	3925	1	150		1115	7

References: 1: Bär et al. (2021), 2: Vogel (2020), 3: Bär (2012), 4: Aretz et al. (2016, 2015) , 5: Stober and Bucher (2015b), 6: Hoth et al. (1997), 7: Sharqawy et al. (2010), 8: Bär et al. (2013), 9: Bär and Sass (2014) and 10: Kastner et al. (2015)

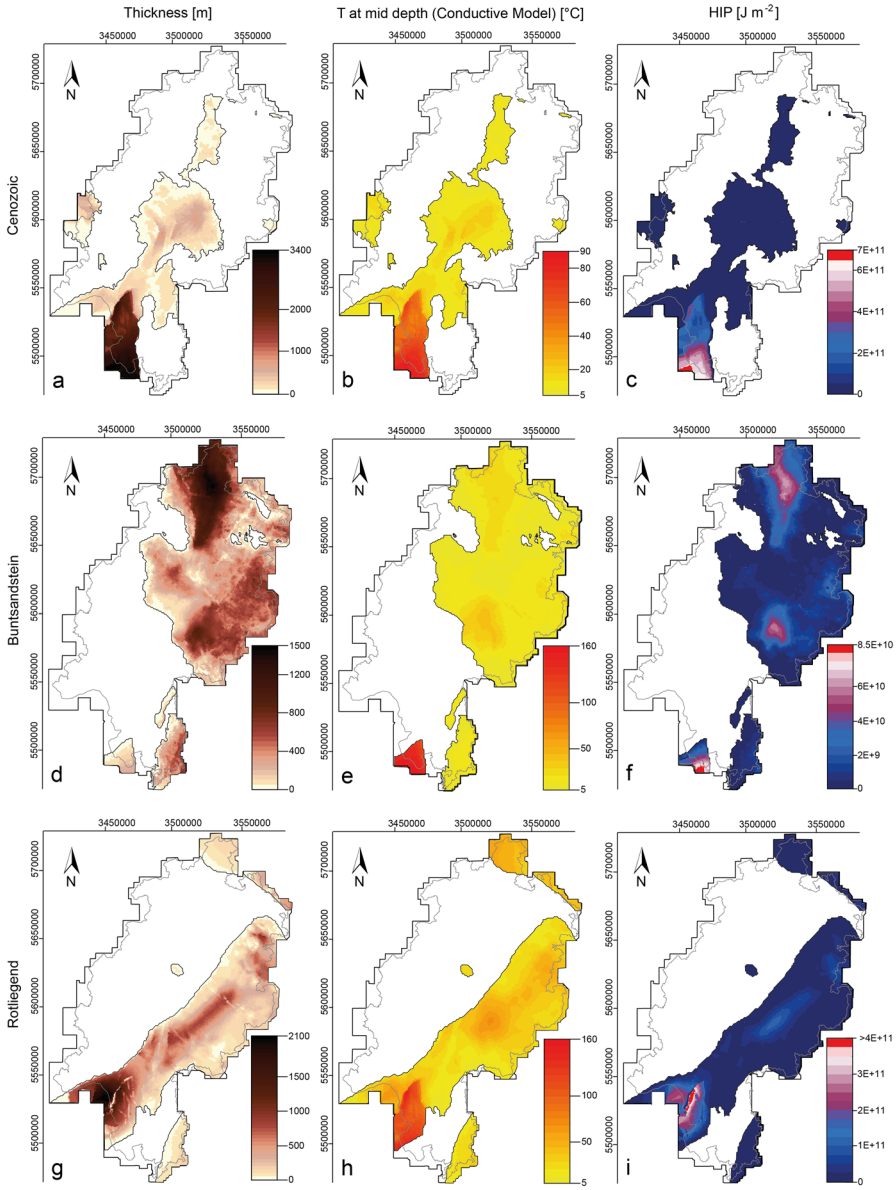

Fig. 2 Results show in columns from left to right thickness distribution and temperature derived with the Conductive Model at the middle reservoir depth [after Koltzer et al. (2019a)] and in the right column calculated HIP values for the three model units of Cenozoic (**a**–**c**), Buntsandstein (**d**–**f**) and Rotliegend (**g**–**i**) from top to bottom. In white regions the respective model unit is missing in the model region. Maps are shown in Gauß–Krüger DHDN Zone 3. Maps were created with ParaView (Squillacote et al. 2007) and the used graphics software was Adobe Illustrator (Adobe Inc. 2019)

well. To follow the main results in this study the structural model and the thermal models are shortly summarized in the following sections. This is complemented by information on input values of rock and fluid properties to calculate the HIP.

Table 2 Geological units (C: Cenozoic, M: Muschelkalk, BS: Buntsandstein, Z: Zechstein, R: Rotliegend, B: Basement) of the structural model (Arndt 2012), with aquifer and aquitard characterization following the parameterization in Koltzer et al. (2019a)

Unit	Aquifer/aquitard	*d* [m]		*t* [m]		T_r conductive model [°C]		T_r advective model [°C]		T_r convective model [°C]	
		Min	Max	Min	Max	Min	Max	Min	Max	Min	Max
C	Aquifer	0	1709	0	3418	5	86	5	125	5	94
M	Aquitard	0	200	0	400	5	35	5	17	5	17
BS	Aquifer	0	3465	0	1472	5	163	5	166	5	110
Z	Aquitard	0	1800	0	977	5	53	5	40	5	40
R	Aquifer	0	3637	0	2107	5	150	5	144	5	103
B	Aquitard	3034	5262	1653	6830	82	207	63	203	69	180

Maps with spatial distribution of the middle depth (*d*) is shown in Additional file 1 of this paper and thickness (*t*) maps are published in Supplementary Material S1 of Koltzer et al. (2019a)

3D structural model of Hesse

Thick sedimentary deposits located mainly in the Hessian Depression in the northeast of Hesse and in the URG in the southwest characterize the subsurface of Hesse (Fig. 1). Arndt (2012) translated the geology of Hesse to a very detailed structural 3D model of Hesse. It integrates more than 100 faults, geological profiles, isoline maps, more than 4000 boreholes, seismic data and several geological maps. The model covers the entire region of the Federal state of Hesse, it extends in north south direction about 250 km and in west east direction 180 km and was built in the modelling software GOCAD (Paradigm 2009). The structural model differentiates six layers. Its upper most five layers are sedimentary deposits and the lower most is the variscan basement. The Cenozoic sediments are the uppermost layer and reach up to 3.4 km thickness in the young rift of the URG (Table 2). Though the Cenozoic sediments are of heterogeneous lithologies with alternating aquifers and aquitards (Lampe and Person 2002; Stober and Bucher 2015b; Hintze et al. 2018; Bär et al. 2021), this unit was characterized as aquifer (Freymark et al. 2019). The unit comprised by the Middle to Upper Triassic (Keuper and Muschelkalk) sediments occurs only very locally, e.g., in grabens where it reaches low thicknesses of up to 400 m and is characterized as an aquitard. The Buntsandstein unit below forms a regional sandstone dominated aquifer (GeORG-Projektteam 2013b; Freymark et al. 2017; Bär 2012; Clauser et al. 2007) and reaches highest thicknesses of up to 1472 m in the north of Hesse in the Hessian Depression (Fig. 1). In the region of the URG, its depth is largest, but the thickness is only up to 260 m. Below the Buntsandstein sediments in the northeast of Hesse the Zechstein aquitard reaches up to 977 m thickness. The deepest sedimentary unit of Early Permian age is the Rotliegend aquifer and is present along the central part of Hesse from the southwest, where it reaches up to 2107 m thickness in the Saar–Nahe Basin and up to 1.5 km thickness in the northern URG (Aretz et al. 2016; Bär 2012). Below the sediments, the metamorphic basement is divided into different Variscan domains (Franke 2000) (Fig. 1b). Of these, the northwestern Rhenohercynian block crops out in the Rhenish Massif (Klügel 1997) and is followed southward by the Northern Phyllite Zone and the Mid German Crystalline High, cropping out in the Odenwald (Stein 2001; Franke 2000; Frey et al. 2021; Weinert et al. 2021).

Thermal models of Hesse

One key parameter for the calculation of naturally stored energy is temperature, which, however, has to be determined for most parts of the deep subsurface through some kind of model since direct measurements from boreholes are generally rare (Arndt et al. 2011). Different thermal models for the deep subsurface of Hesse (and surrounding regions) have been developed in recent years which implement existing borehole temperatures either directly by interpolating the thermal field between them (Arndt et al. 2011, 2012; Agemar et al. 2012; Rühaak et al. 2014) or by using them to validate heat transport models (e.g. Freymark et al. 2015, 2017). None of these models, however, have considered the effects of regional groundwater flow on deep temperature although fluid transport is known to exert an important contribution to thermal anomalies in the northern Upper Rhine Graben (URG; e.g. Bär, 2012; Clauser et al. 2002; Koltzer et al. 2019a, Fig. 1). To quantify these effects for the entire state of Hesse was the objective of Koltzer et al. (2019a) who therefore conducted investigations based on hydraulic, thermal and coupled thermo-hydraulic numerical simulations applied to the 3D geological model of Hesse (Arndt et al. 2011). All model scenarios were compared with temperature data from 467 boreholes to prove the quality of the model (Koltzer et al. 2019a). All vertical boundaries were closed for fluid flow and heat transport. At the surface Dirichlet boundary conditions were set for constant hydraulic head equal to the groundwater surface after Herrmann (2010) and constant temperature (DWD 2013). The boundary at the bottom of the model was closed for fluid flow and a Dirichlet constant temperature distribution exported from the lithospheric-scale model of Freymark et al. (2017) was applied. The different temperature distributions obtained from these simulations are used in the present study to derive different scenarios for HIP calculations. Accordingly, we will discuss the different HIP scenarios based on three different temperature distributions from the respective thermal models: (I) a purely conductive thermal model (Conductive Model), (II) a coupled hydrothermal steady-state model (Advective Model) and (III) a hydrothermal transient model at a state after a simulation time of 100,000 years (Convective Model). We treat the model realizations as equally plausible scenarios in terms of their temperature variations since (i) a comparison with the available borehole temperatures does not give clear evidence in favor of one model over another (Koltzer et al. 2019a) and (ii) prospectively we will need to augment our understanding of the interplay of all temperature controlling mechanisms at depth to improve our predictive models.

Based on the structural 3D model of Arndt (2012), Rühaak et al. (2014) generated a numerical mesh with FEFLOW© (Diersch 2014) to simulate conductive heat transport in Hesse. Koltzer et al. (2019a) adopted the numerical mesh of Rühaak et al. (2014) with a high horizontal resolution of 1 km, increasing locally to less than 100 m. The six geological layers are represented in 21 numerical layers with thicknesses varying between 1.1 km and 10 m. All relevant equations of the processes of conduction, advection and convection with simulations of different degrees of physical complexity were solved with the modelling software FEFLOW© (Diersch 2014). For model simplification, all rock properties for the hydraulic, thermal and thermohydraulic numerical simulations were considered constant and homogeneous as listed in Table 2 of Koltzer et al. (2019a). The simulation results were compared to hydraulic, hydrochemical and temperature data to

describe regions, where the model can reproduce observations and regions where higher resolution or more input data would be needed. By stepwise coupling of thermal and hydraulic processes in thee simulations, Koltzer et al. (2019a) could identify domains in Hesse dominated by different heat transport mechanisms.

The conductive heat transport dominates regions with low hydraulic conductivity, the region of the Rhenish Massif and Odenwald, were the basement crops out (Koltzer et al. 2019a). In general, highest temperatures are predicted with the Conductive Model. As this model is physically less complex and fundamental, we use this model for a first calculation of the HIP to generally describe the trends of high and low prospective areas. The influences of advection and convection are discussed subsequently.

The infiltration of cold groundwater into more permeable sedimentary layers described as the advective heat transport in Koltzer et al. (2019a), cools down the conductive thermal field in regions were high hydraulic gradients are predicted. This is the case for example in the Hessian Depression in the north and along the Eastern Main Border Fault of the URG in the south. The steady state thermohydraulic model, considering the influence of pressure driven fluid flow on the conductive thermal field is referred to as the "Advective Model" in this work.

The third process of heat convection perturbs the advective hydrothermal field of Hesse additionally only in the region of the URG. This (fluid-density-driven) convection-dominated domain is characterized by permeable layers of the Rotliegend, Buntsandstein and Cenozoic with high thicknesses (Fig. 2), high geothermal gradients as consequence of high heat input from the crystalline basement below the graben, the presence of isolating sediments in the graben (Freymark et al. 2015, 2017) and low hydraulic gradients in the valley (Koltzer et al. 2019a). The fully coupled transient thermohydraulic model, which solves not only for conduction and advection but also for buoyancy-forced free convection is referred to as "Convective Model" in this study.

Parametrization of the HIP calculations

To close the system of equations the prescription of boundary conditions is required. Therefore, we used the annual mean temperature as reference temperature at the surface (DWD 2013) to be consistent with the numerical models, where this surface temperature distribution is used as upper Dirichlet boundary condition (Koltzer et al. 2019a). The reservoir temperature for the calculation of the HIP was extracted for each reservoir unit at the middle vertical depth of the three thermal models: the Conductive, Advective and Convective Model according to Eq. 2 (Additional file 1: Fig. S1):

$$d = d_{\text{top}} - \frac{t}{2} \tag{2}$$

The middle reservoir depth (d, Eq. 2, Additional file 1: Fig. S1), is the calculated z-value for each X/Y-grid point in the numerical mesh. d_{top} is the top of the respective reservoir unit and t is the thickness of the reservoir unit.

In our HIP calculation, we consider the total thickness of the respective geological unit for the volume calculation. For model simplification, we assume the geological units to be homogeneous in terms of all relevant rock properties and list the respective constant values in Table 1. The specific heat capacity of the solid parts of the

rocks ($c_{\mathrm{p,m},T_\mathrm{r}}$) was calculated by converting a value at standard conditions ($c_{\mathrm{p,m},T_{20}}$) to reservoir temperature conditions using existing approximation equations for sedimentary rocks (Eq. 3) and for metamorphic basement rocks (Eq. 4), respectively, modified by Bär (2012) after Vosteen and Schellschmidt (2003):

$$c_{\mathrm{p,m},T_\mathrm{r}} = 6.295 \cdot 10^{-6} \cdot T_\mathrm{r}^3 - 4.99 \cdot 10^{-3} \cdot T_\mathrm{r}^2 + 1.71 \cdot T_\mathrm{r} + c_{\mathrm{p,m},T_{20}} \tag{3}$$

$$c_{\mathrm{p,m},T_\mathrm{r}} = 5.389 \cdot 10^{-6} \cdot T_\mathrm{r}^3 - 4.648 \cdot 10^{-3} \cdot T_\mathrm{r}^2 + 1.70 \cdot T_\mathrm{r} + c_{\mathrm{p,m},T_{20}} \tag{4}$$

The heat capacity of the fluid is considered to be constant as described in Bär et al. (2021), the pressure effect decreases with increasing salinity and with different equations to correct for temperature effects after Knoebel et al. (1968); Jamieson et al. (1969); Nayar et al. (2016), who conclude that a constant value for the heat capacity of the fluid is acceptable as consequence of very low variation.

The density of the pore fluid (ρ_f) is dependent on its salinity (S), temperature and pressure (p). To calculate the density of the pore fluid under reservoir conditions we used the empirical equation of Batzle and Wang (1992), which is valid under the reservoir conditions in Hesse (Bär et al. 2021). Therefore, beside the reservoir temperature also the hydraulic pressure at the middle depth of the geological unit was estimated (Eq. 5):

$$p = \rho_{\mathrm{f},T_{20}} \cdot g \cdot d + p_\mathrm{atm} \tag{5}$$

With $\rho_{\mathrm{f},T_{20}}$ as fluid density at 20 °C dependent on the salinity [Table 1, Sharqawy et al. (2010)], g the gravity, p_atm the atmospheric pressure (101325 Pa).

Then, we correct the density of fresh water (ρ_fw) according to the reservoir temperature and pressure with Eq. 6:

$$\begin{aligned}\rho_\mathrm{fw} =& 1 + 10^{-6} \cdot \Big(-80T_\mathrm{r} - 3.3T_\mathrm{r}^2 + 0.00175T_\mathrm{r}^3 + 489p - 2T_\mathrm{r}p + 0.016T_\mathrm{r}^2p \\ & -1.3 \cdot 10^{-5}T_\mathrm{r}^3p - 0.333p^2 - 0.002T_\mathrm{r}p^2\Big)\end{aligned} \tag{6}$$

In a final step, we correct for salinity with Eq. 7:

$$\rho_\mathrm{f} = \rho_\mathrm{fw} + S \cdot \Big(0.668 + 0.44S + 1 \cdot 10^{-6} \cdot (300p - 2400pS + T_\mathrm{r} \cdot (80 + 3T_\mathrm{r} - 3300S - 13p + 47pS))\Big) \tag{7}$$

Calculated HIP variations in the model units beneath Hesse

The results of this study focus on the HIP prediction of the three aquifer units (after Koltzer et al. 2019a), as for these units the highest values for HIP are predicted. The results of the units characterized as aquitards (Basement, Zechstein and Muschelkalk) are published in Additional file 2 for completeness. In the following the predicted HIP in GJ m^{-2} is presented as a consequence of the combined variations in unit thickness and temperatures.

Our predictions rely on complex thermo-hydraulic temperature models which commonly predict lower temperatures in all three reservoir units outside the URG. This translates in highest values of HIP inside the URG. Therefore, this region will be in focus of the result assessment. Inside the graben sediments the calculated HIP shows systematic spatial variations in some reservoirs. In the Cenozoic and Buntsandstein the

thickness and the temperature increase from north to south. This trend leads to a similar pattern of increasing HIP from north to south in both units (Fig. 2). In this section, we will investigate how the thickness of each unit in combination with the temperature influence the predicted HIP. To illustrate the temperature influences without effects of fluid flow in this first set of results, we describe first the temperatures predicted by the Conductive Model as a reference model (Fig. 2).

The temperature is the main process-dependent input parameter for the calculation of the HIP, and in the same way this input defines tremendously the amount of predicted HIP. Koltzer et al. (2019a) showed the influence of different heat transport mechanism on the predicted thermal fields and following this approach we investigate in the second step the differences of calculated HIP variations based on different heat transport models. Therefore, the HIP calculated based on the Advective and Convective Model are illustrated as difference maps to the HIP based on the Conductive Model (Fig. 3). In most regions, temperatures and HIPs are highest for the Conductive Model, but some regions are affected by upwelling hot fluids leading to higher predicted HIP for the Advective and the Convective Models (red regions in Fig. 3).

HIP of the Cenozoic

The Cenozoic reaches very high thicknesses between 1.5 and 3.4 km in the URG. In the region outside the graben the thickness is lower with less than 1 km (Fig. 2a). Predicted temperatures are highest with the Conductive Model and vary between 40 and 86 °C at a middle reservoir depth of 1.6 km in the central URG and lower temperatures between 5 and 25 °C outside the URG.

The predicted HIP for the Cenozoic unit is predicted to be very low (up to 30 GJ m^{-2} with the Conductive Model) in Hesse outside the region of the URG. In the URG the HIP is predicted to be highest in the southernmost and northwesternmost parts of the URG ranging from 130 to 700 GJ m^{-2} (Fig. 2c).

In summary, the HIP is highest in the model unit of Cenozoic inside the URG. There, the effect of freshwater infiltration in regions affected by advective heat transport is visible in the HIP differences between the HIP based on the Conductive and the Advective Model. With the Advective Model the HIP is predicted to be about 360 GJ m^{-2} lower in contrast to the Conductive Model along the Eastern Main Border Fault. On the other hand, pressure driven fluid flow leads to locally up to 310 GJ m^{-2} higher predicted HIP in the western half of the URG of (Fig. 3a). The difference between predictions of HIP based on the Conductive minus the HIP based on the Convective Model, illustrate that the heat transport by free convection leads to locally up to 540 GJ m^{-2} lower predicted HIP in the URG and locally up to 95 GJ m^{-2} higher predicted HIP (Fig. 3b). Along the northern region of the Western Main Border Fault of the URG the HIP is predicted to be up to 70 GJ m^{-2} higher based on the Advective and Convective Models (Fig. 3a, b) than predicted by the Conductive Model.

In general, high HIP values in the URG are spatially more restricted with the predictions based on the Advective Model to the western side of the URG. The difference map between the HIP derived based on the Conductive and the Convective Model makes the locally higher predicted HIP in the URG visible. Thereby, the high HIP is restricted to

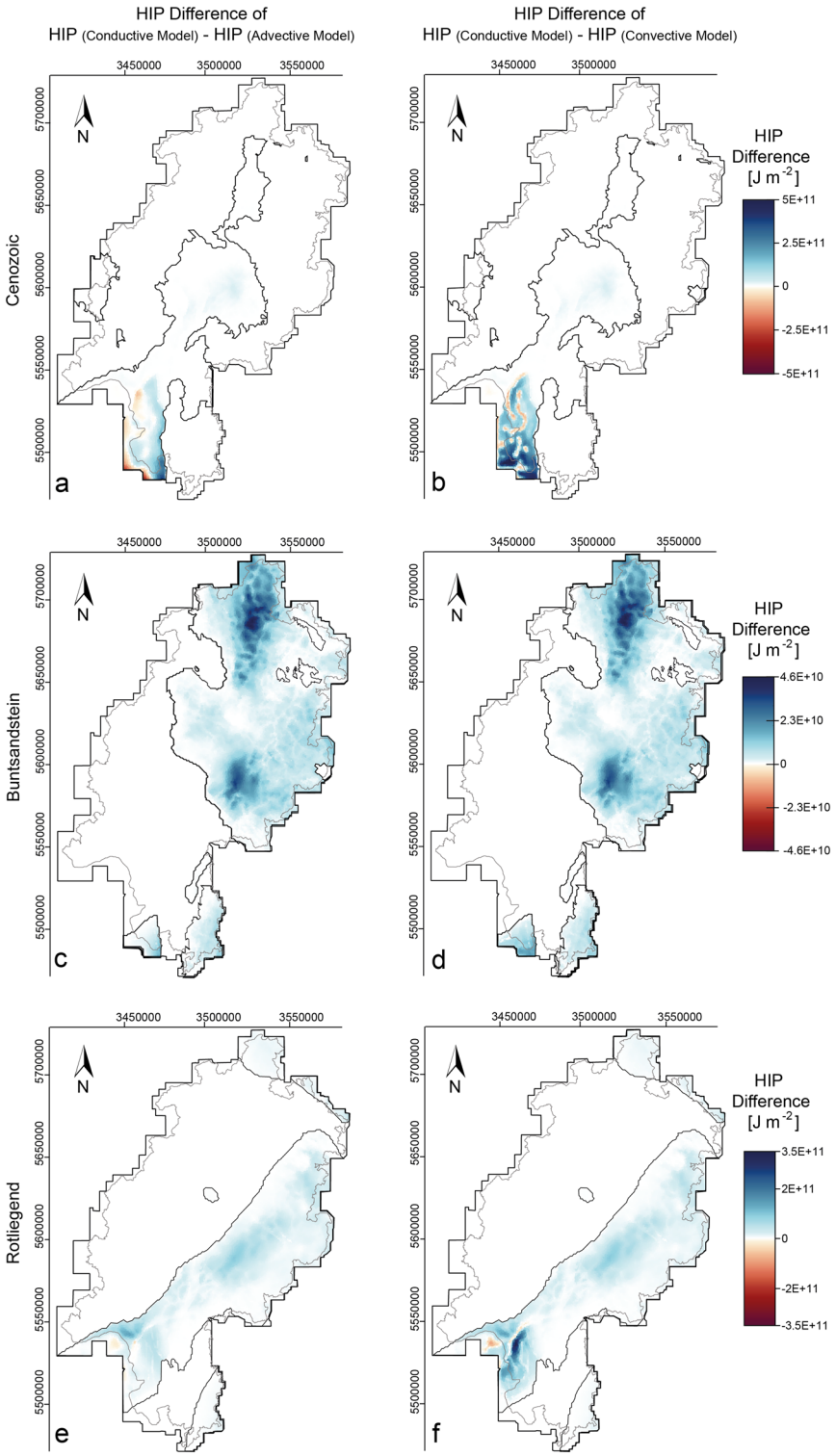

Fig. 3 Difference maps of the HIP in the Cenozoic (**a**, **b**), Buntsandstein (**c**, **d**) and Rotliegend (**e**, **f**) model units from top to bottom. The HIP differences show the calculated HIP from the Conductive Model minus the Advective Model (**a**, **c**, **e**) and the calculated difference of the Conductive Model minus the Convective Model (**b**, **d**, **f**). With blue colours lower HIP is predicted with the Advective and Convective Models and with red colours, advection and convection lead to higher predicted HIP. Maps are shown in Gauß–Krüger DHDN Zone 3. Maps were created with ParaView (Squillacote et al. 2007) and the used graphics software was Adobe Illustrator (Adobe Inc. 2019)

even smaller zones in the Convective case, than based on the Advective Model. Highest values of HIP based on the Convective Model correlate with resolved thermal anomalies, though of higher magnitudes than for the Conductive and Advective Models. The comparison between HIP based on the different heat transport model realizations illustrates that the consideration of all relevant coupled transport processes (conductive, advective and convective heat transport mechanisms) lead to a general net decrease in HIP on a regional scale (blue region in Fig. 3a, b) and only very locally to a HIP increase in the URG.

HIP of the Buntsandstein

The Buntsandstein deposits are mainly encountered in two distinct areas of Hesse, the Hessian Depression in the north and the URG in the south. In the Hessian Depression highest thicknesses of up to 1.5 km are found for the Buntsandstein (Fig. 2d). The unit there is characterized by a low burial depth. On the contrary the Buntsandstein deposits in the URG reach only thicknesses of up to 250 m but are located at a middle depth of nearly 3.5 km.

This geological configuration leads to low temperatures in the Hessian depression of about 30 °C at a maximum depth of 800 m predicted based on the Conductive Model and to high temperatures in the URG of up to 166 °C. The measurements in Kassel–Wilhelmshöhe in the Hessian Depression confirm these low predicted temperatures in the Hessian Depression with 33 °C at a depth of 800 m below the surface and an overall lower geothermal gradient of 26 °C km^{-1}.

The HIP calculated for the Buntsandstein is high in the Hessian Depression as well as in the URG with highest values of 85 GJ m^{-2}. It is the combined effect of (i) high temperatures in the URG and (ii) high thickness in the Hessian Depression that leads to high HIP in both areas.

In the area of the Hessian Depression the predicted HIP in the Buntsandstein based on the Advective Model is reduced by up to 45 GJ m^{-2}, which is about 65% of the entire HIP in the Hessian Depression (Fig. 3c). The reduction is mainly caused by temperature decreases due to cold freshwater infiltration. This effect is observed along the Eastern Main Border Fault of the URG as well.

The difference maps of the Convective and Advective Models with the Conductive Model are identical in the Hessian Depression, though the convection has no influence on the HIP of the Buntsandstein there. This is not surprising, as this region is influenced by advective heat transfer, with no influence of free convection (Koltzer et al. 2019a). Only locally in the Buntsandstein sediments in the URG we detect a difference between the predicted HIP based on the Advective and Convective Models with a slightly lower predicted HIP based on the most complex Convective Model (Fig. 3d).

HIP of the Rotliegend

Rotliegend sediments comprise the deepest sedimentary (and volcanic) geothermal reservoir in Hesse. Hence, they are structurally characterized by the largest reservoir middle depths of up to 3.6 km below surface along the northern most part of the Western Main Border Fault in the URG. There they reach thicknesses of up to 1.9 km. In the deposits of the Hessian part of the Saar–Nahe Basin, Rotliegend sediments reach up to

2.1 km, there the middle reservoir depth is shallower at up to 1.3 km below surface. In the other regions of Hesse the thickness is less than 900 m. The two regions (Saar–Nahe Basin and URG) are most promising for geothermal utilization of the Rotliegend unit.

In the URG, temperatures of 80 °C to 150 °C are predicted with the Conductive Model, with highest temperatures along the Western Main Border Fault. In the Saar–Nahe Basin temperatures range from 20 to 65 °C. This leads to highest predicted HIP in the URG 617 GJ m^{-2} along the Western Main Border Fault, where the thickness as well as the temperature are highest in the URG region. In the Saar–Nahe Basin the HIP is predicted to be only less than half as high as in the URG with up to 270 GJ m^{-2}, and, though the thickness there is higher than in the URG, the temperatures are lower (Fig. 2e, f).

In summary, the predicted HIP for the Rotliegend lies in the same range like the values obtained for the Cenozoic. In the URG the HIP is predicted to be 83 GJ m^{-2} lower in the Rotliegend than in the Cenozoic based on predictions of the purely conductive thermal field.

In the URG highest temperatures are predicted with the Conductive, moderate temperatures with the Advective and lowest temperatures with the Convective Model. Based on the temperature differences between the three thermal models we observe an overall cooling effect by solving for advection and convection in addition to pure conduction (Koltzer et al. 2019a). This leads to a lower predicted HIP of the Rotliegend reservoir based on the Advective Model up to 617 GJ m^{-2}, a reduction that amounts about 55 GJ m^{-2} in the URG. In the Saar–Nahe Basin, the HIP is reduced even more by 100 GJ m^{-2} to a total amount of 270 GJ m^{-2} (blue in Fig. 3e). The process of rising hot fluids driven by buoyancy forces represented in the Convective Model lead to locally higher temperatures along the Western Main Border Fault of the URG and in the Saar–Nahe Basin. This also leads to higher predicted HIP of about 26 GJ m^{-2} in the URG and of about 86 GJ m^{-2} in the Saar–Nahe Basin (reddish in Fig. 3f).

Discussion

Before discussing the results in this section, it is necessary to pin point some limitations of the calculated HIP. As for any model, there are uncertainties and a limited resolution in the basic geological model (Arndt et al. 2011; Van Der Vaart et al. 2021) as well as in the thermal models [discussed in Koltzer et al. (2019a)]. Also the limitations related to the choice of parameters (physical properties and boundary conditions) set to derive the HIP need to be mentioned. The more detailed modelling is allowed by the available data for reservoir characterization, the more precise can the prediction of HIP be. With the example of the salinity in the pore fluid, we will demonstrate the importance of site-specific properties and how the predictions of the exact values of HIP are sensitive to the fluid salinity explicitly for one local area. Higher salinity of the fluid leads to much higher density of the fluid, which in the end leads to significantly increased values of the HIP. In the regional scale quantification, as considered in this study, it is reasonable to use mean values to quantify the HIP at this scale and to investigate the influences of fluid flow and heat transport processes on the predictions. In more local studies or for an actual prospection of geothermal resources, more detailed geological models and more sophisticated model parametrizations are required.

In the Zechstein unit, the parameterization of salinity is complicated, caused by highly heterogeneous lithologies from dolomite to pure salt (Bär 2012), which cannot be incorporated accurately in a regional scale model. However, low salinities of 34 g l^{-1} [mean values from the new data base by Schäffer et al. (2020, 2021)] and very high salinities of 443 g l^{-1} [mean values for Hesse by Ludwig (2013)] were both tested as endmembers for the fluid composition and properties. The resulting HIP calculated with different salinity varies only up to 2%, therefore it can be concluded that the exact knowledge of the salinity of the geothermal reservoir has a subordinate relevance for regional predictions of HIP compared to thickness, temperature or porosity.

Thickness vs. temperature effects on the HIP in Hesse

For all model units, calculated HIP is highest in the URG. Based on these results, we can subdivide the area of Hesse in two different domains: (I) a high prospective target domain in the URG and (II) a low prospective domain elsewhere.

In addition, the predictions of the HIP point to a highly promising region in the northwestern part of the URG along the Western Graben Border Fault. There, Cenozoic and Rotliegend sediments reach largest thicknesses and HIP is predicted to be very high in this region. This is true not only for the HIP predicted based on the Conductive Model, but also based on the Advective and Convective Models as both fluid assisted heat transport processes lead to predictions of higher temperatures in locally restricted upflow zones of hot fluids in this area. Additional support for these findings, comes from a study of Bär (2012) showing that this area coincides spatially with the predicted distribution of largest hydrothermal potentials for the Rotliegend reservoir.

Mostly due to their relatively small thicknesses, Muschelkalk and Zechstein are characterized by the lowest HIP values ("Muschelkalk and Keuper, Zechstein" section). As they are generally regarded as aquitards these units should be of little interest for deep geothermal energy (Bär 2012). For this reason, we concentrate our discussion on more promising geological units here, i.e. the hydraulically more conductive and thicker Cenozoic, Buntsandstein and Rotliegend model units.

While for the Cenozoic and Rotliegend geological units both the predicted temperatures and the HIP are highest in the URG, for the Buntsandstein predicted HIP values are similarly large in the Hessian Depression, where overall lower temperatures prevail than in the URG. This is because of the larger thicknesses of the Buntsandstein unit in the northern part of the study area. The temperature differences between the purely conductive and the coupled fluid and heat transport models, however, relativize the thickness effect: stronger recharge of cold surface waters may strongly lower the temperatures and therefore the HIP values in the North of our study area despite of an increasing thickness of the unit. Combining these results of moderately high HIP in the Hessian Depression with the conclusion, that this region is highly influenced by the groundwater flow Koltzer et al. (2019a) indicates that the region of the Hessian Depression is more suitable for shallow geothermal applications, as also suggested by e.g. Lund (2018); Antics and Sanner (2007). Moreover, seasonal energy storage as e.g. aquifer thermal energy storage (ATES) Vogel (2020); Bär et al. (2021) should be considered as an appropriate application in the Hessian Depression. As Germany is located in a climate zone, where

both heating and cooling is needed (Bloemendal et al. 2015), we recommend that a more detailed explorative study of the heat storage capacity in the Buntsandstein is required at this stage.

Going one step further and addressing the influence of thickness and temperature distribution in a sensitivity analysis and an uncertainty quantification could be done in future work.

Influences of physical transport processes on the HIP

There are different processes and mechanisms influencing the predicted HIP, which have to be considered when geothermal resources are assessed. In this study, we investigate how the level of complexity in subsurface hydrothermal dynamics influences the predicted HIP. Depending on the underlying heat transport mechanisms considered the predicted HIP can vary in each model unit. The predicted heating power is found to be the highest for all units under the assumption of conductive heat transport conditions. This is not surprising, given the conclusions drawn in Koltzer et al. (2019a) that advective heat transport leads to a net cooling of the system by surface water infiltration, reaching deeper into the aquifers following the main topography gradients. This process is most pronounced in specific areas characterized by high hydraulic gradients in units of high hydraulic conductivity. Consequently, this process leads to lower calculated HIP in advective influenced regions (e.g. in the Hessian Depression and along the the Eastern Graben Border Fault of the URG Fig. 3a–c). The extent of this effect might however be overestimated in our models, due to their simplified geometry and homogeneous parametrisation. Especially in layered sediments, a strong anisotropy of the hydraulic conductivity is well known, so that the horizontal hydraulic conductivity is usually one to two orders of magnitude higher than in the vertical direction. Additionally, the model units of the Cenozoic, Buntsandstein and Rotliegend have to be considered as a layered succession of aquifers and aquitards, where only the aquifers show properties characterizing them as geothermal reservoirs. Thus, the depth and impact of vertical infiltration of cold surface waters might be overestimated in our models [discussed in more detail in Koltzer et al. (2019a)].

Taking the Conductive Model as a reference model, as this is most commonly state of the art for predicting the thermal field on a regional scale (Limberger et al. 2018; Magri et al. 2014; Freymark et al. 2015, 2017; Rühaak et al. 2014; Bär 2012; Arndt 2012; Noack et al. 2012; Bonté et al. 2012), looking at the differences in temperature and HIP predictions by considering also free convective heat transport leads to additional positive and negative influences. Accordingly, local positive thermal anomalies occurring in the URG (e.g. Pribnow and Clauser 2000) correspond to an increased predicted HIP (Fig. 3b, f). Due to convective fluid circulation and associated thermal anomalies characteristic for the system only in the northern part of the URG, the predicted HIP vary over short lateral distances. On the other hand, free convection in the URG also has the highest negative impact on the predicted stored heat. For example, in the Rotliegend, the HIP is predicted to be reduced by 350 GJ m^{-2} for the Convective Model which is about the half of the highest predicted HIP in this unit for the reference (Conductive) Model, and locally by 570 GJ m^{-2} in the Cenozoic (Fig. 3b, f).

This huge amount of positive and negative differences underlines the importance of correct temperature predictions before predicting any kind of geothermal potentials. Here it is of special importance to always calibrate any kind of temperature models by all subsurface temperature measurements available to ensure that the modelled processes are in accordance with in-situ observations. Moreover, this visualizes, the high risks of drilling deep geothermal wells into convectively influenced reservoirs, where the well can either hit a positive geothermal anomaly or is drilled beside it resulting in much lower observed temperatures.

Future work should focus on the area of the URG as this is the most prospective but also one of the geologically most complex areas for geothermal energy production in Hesse. There, the potential of different applications should be tested, but being always aware of the high importance of positive and negative thermal anomalies caused by the process of convective heat circulation. Therefore, the key target for geothermal exploration is to correctly locate positive geothermal anomalies in the subsurface (Bär et al. 2020).

Conclusions

With this study, we could show how the different heat transport mechanisms influence the predicted geothermal potential by applying the "heat in place" (HIP) method. Considering complex 3D physical process simulations as a basis for a fundamental methodological approach to predict geothermal potentials make it possible to quantify the influence from different heat transport processes on the predicted HIP. Consequently, this study emphasizes the need to understand physical processes at different spatial and time scales to make at first meaningful temperature predictions (Scheck-Wenderoth et al. 2017) and—based on those—precise predictions of HIP or technical or economical geothermal potentials.

The size and extent of highly prospective areas identified based on the thermal models (Koltzer et al. 2019a) can be further specified through the HIP calculations.

Our limited knowledge about the existence, size and extent of fluid convection cells in the porous aquifers of the URG (Bär et al. 2020) leads to a high uncertainty in the estimation of locally stored (and producible) energy. This illustrates the need for further exploration measures for local geothermal projects. Before considering utilization of the heat, it is necessary to estimate the geothermal potential in the targeted region more precisely by quantifying the recoverable heat (Garg and Combs 2015; Dalla Longa et al. 2020).

In general, an overall trend can be described, that predicted HIP derived from temperatures based on purely conductive thermal models are highest and that the predicted geothermal potential is reduced when advection and free convection are included in the models. This reduction highlights the importance to investigate the fluid flow processes in combination with heat transport and their impact on the prediction of the HIP, especially in sedimentary reservoirs where fluid circulation can play a major role in the heat transport processes.

Abbreviations

URG Upper Rhine Graben

HIP	Heat in place
ECRS	European Cenozoic Rift System
NGB	North German Basin
H	Stored heat
V	Volume
ρ	Density
m	Rock matrix
f	Pore fluid
φ	Porosity
T	Temperature
r	Reservoir
ref	Reference
d	Middle reservoir depth
t	Thickness
$c_{\mathrm{p,m},T_\mathrm{r}}$	Specific heat capacity of the rock matrix under reservoir temperature
$c_{\mathrm{p,m},T_{20}}$	Specific heat capacity of the rock matrix at 20 °C
$c_{\mathrm{p,f}}$	Specific heat capacity of the fluid
ρ_f	Density of the pore fluid
S	Salinity
p	Pressure
$\rho_{\mathrm{f},T_{20}}$	Fluid density at 20 °C
p_atm	Atmospheric pressure
g	Gravity
ρ_fw	Density of fresh water

Supplementary Information

The online version contains supplementary material available at https://doi.org/10.1186/s40517-023-00245-7.

Additional file 1. Middle depth of model units.

Additional file 2. Temperature and HIP of low permeable units.

Acknowledgements
We want to thank the three anonymous reviewers for their contributions which helped improve the quality of this manuscript. We kindly acknowledge DHI WASY for the sponsored MIKE Powered by DHI license files. Thank you to Wolfram Rühaak, providing the basic Feflow model. Furthermore, we are thankful for all provided data by the HLNUG.

Author contributions
NK prepared the input data and calculated the HIP for all units with the python code, NK created the figures and was the major contributor in writing the manuscript. JB supported NK during the calculation of the HIP in python. All authors read and approved the final manuscript.

Funding
Open Access funding enabled and organized by Projekt DEAL. The Federal Ministry for Economic Affairs and Climate Action (BMWK) is gratefully acknowledged for economic support through the research project "Hessen-3D II: 3D-Modellierung der geothermischen Tiefenpotenziale von Hessen", coordinated by the Technical University of Darmstadt (Grant Agreement Nos. 0325944 A and 0325944 B).

Declarations

Availability of data and materials
The data sets used to calculate the HIP during the current study are available from the corresponding author on reasonable request.

Competing interests
The authors declare that they have no competing interests.

Received: 2 March 2022 Accepted: 31 December 2022
Published online: 27 January 2023

References

Adobe Inc. Adobe illustrator; 2019. https://adobe.com/products/illustrator.
Agemar T, Schellschmidt R, Schulz R. Subsurface temperature distribution in Germany. Geothermics. 2012;44:65–77. https://doi.org/10.1016/j.geothermics.2012.07.002.
Antics M, Sanner B. Status of geothermal energy use and resources in Europe. In: Proceedings European geothermal congress 2007, Unterhaching, Germany; 2007.

Aravena D, Muñoz M, Morata D, Lahsen A, Parada MA, Dobson P. Assessment of high enthalpy geothermal resources and promising areas of Chile. Geothermics. 2016;59:1–13. https://doi.org/10.1016/j.geothermics.2015.09.001.
Aretz A, Bär K, Götz AE, Sass I. Facies and diagenesis of permocarboniferous geothermal reservoir formations (Upper Rhine Graben, SW Germany): impact on thermophysical and hydraulic properties. In: Proceedings world geothermal congress, Melbourne; 2015.
Aretz A, Bär K, Götz AE, Sass I. Outcrop analogue study of permocarboniferous geothermal sandstone reservoir formations (northern Upper Rhine Graben, Germany): impact of mineral content, depositional environment and diagenesis on petrophysical properties. Int J Earth Sci. 2016;105:1431–52. https://doi.org/10.1007/s00531-015-1263-2.
Arndt D. Geologische strukturmodellierung von hessen zur bestimmung von geopotenzialen. PhD thesis, Technische Universität Darmstadt, Germany; 2012.
Arndt D, Bär K, Fritsche J-G, Kracht M, Sass I, Hoppe I. 3D structural model of the Federal State of Hesse (Germany) for geopotential evaluation [Geologisches 3D-modell von hessen zur bestimmung von geo-potenzialen]. Zeitschrift der Deutschen Gesellschaft für Geowissenschaften. 2011;162:353–69. https://doi.org/10.1127/1860-1804/2011/0162-0353.
Bär K. Untersuchung der tiefengeothermischen potenziale von hessen. PhD thesis, Technische Universität Darmstadt, Germany; 2012.
Bär K, Sass I. 3D-model of the deep geothermal potentials of Hesse (Germany) for enhanced geothermal systems. In: Thirty-ninth workshop on geothermal reservoir engineering Stanford University, Stanford, California; 2014.
Bär K, Arndt D, Fritsche J-G, Götz AE, Kracht M, Hoppe A, Sass I. 3D-modellierung der tiefengeothermischen potenziale von hessen - eingangsdaten und potenzialausweisung [3D modelling of the deep geothermalpotential of the federal state of Hesse (Germany)—input data and identification of potential]. Zeitschrift der Deutschen Gesellschaft für Geowissenschaften. 2011;162:371–88. https://doi.org/10.1127/1860-1804/2011/0162-0371.
Bär K, Arndt D, Hoppe A, Sass I. Investigation of the deep geothermal potentials of Hesse (Germany). Pisa: European Geothermal Congress; 2013.
Bär K, Reinsch T, Bott J, Cacace M, Frey M, Van Der Vaart J, Scheck-Wenderoth M, Ritter O, Homuth B, Fritsche J-G, Spath F, Sass I. Integrated exploration strategy 'convex' to detect hydrothermal convection in the subsurface. In: Proceedings world geothermal congress, Reykjavik, Iceland; 2020.
Bär K, Schäffer R, Weinert S, Sass I. Verbundprojekt "hessen 3D 2.0" 3D-modell der geothermischen tiefenpotenziale von hessen - petrothermale potenziale und mitteltiefe potenziale zur wärmenutzung und wärmespeicherung (teilvorhaben a). Schlussbericht zum bmwi-geförderten verbundprojekt "hessen 3D 2.0" (fkz 0325944a); 2021.
Batzle M, Wang Z. Seismic properties of pore fluids. Geophysics. 1992. https://doi.org/10.1190/1.1443207.
Bèdard K, Comeau FA, Raymond J, Gloaguen E, Malo M, Richard M-A. Deep geothermal resource assessment of the St. Lawrence Lowlands sedimentary basin (Québec) based on 3D regional geological modelling. Geomech Geophys Geo-Energy Geo-Resour. 2020. https://doi.org/10.1007/s40948-020-00170-0.
Bloemendal M, Olsthoorn T, van de Venad F. Combining climatic and geo-hydrological preconditions as a method to determine world potential for aquifer thermal energy storage. Sci Tot Environ. 2015;538:621–33. https://doi.org/10.1016/j.scitotenv.2015.07.084.
Bonté D, van Wees J-D, Verweij JM. Subsurface temperature of the onshore Netherlands: new temperature dataset and modelling. Neth J Geosci (Geologie en Mijnbouw). 2012;91:491–515.
Bott J, Benoit L, Koltzer N, Anikiev D. Py4hip—python script for heat-in-place calculations. GFZ Data Publ. 2022. https://doi.org/10.5880/GFZ.4.5.2022.001.
Bracke R, Huenges E, Acksel D, Amann F, Bremer J, Bruhn D, Bussmann G, Görke U-J, Grün G, Hahn F, Hanßke A, Kohl T, Kolditz O, Regenspurg S, Reinsch T, Rink K, Sass I, Schill E, Schneider C, Shao H, Teza D, Thien L, Utri M, Will H. Roadmap tiefe geothermie für deutschland: Handlungsempfehlungen für politik, wirtschaft und wissenschaft für eine erfolgreiche wärmewende. strategiepapier von sechs einrichtungen der fraunhofer-gesellschaft und der helmholtz-gemeinschaft; fraunhofer-einrichtung für energieinfrastrukturen und geothermie (ieg), fraunhofer-institut für umwelt-, sicherheits- und energietechnik (umsicht), fraunhofer-institut für bauphysik (ibp), helmholtz-zentrum potsdam deutsches geoforschungszentrum (gfz), karlsruher institut für technologie (kit), helmholtz-zentrum für umweltforschung (ufz); 2022.
Calcagno P, Baujard C, Guillou-Frottier L, Dagallier A, Genter A. Estimation of the deep geothermal potential within the Tertiary Limagne basin (French Massif Central): an integrated 3D geological and thermal approach. Geothermics. 2014;51:496–508. https://doi.org/10.1016/j.geothermics.2014.02.002.
Clauser C, Griesshaber E, Neugebauer HJ. Decoupled thermal and mantle helium anomalies: implications for the transport regime in continental rift zones. J Geophys Res Solid Earth. 2002;107:2269. https://doi.org/10.1029/2001JB000675.
Clauser C, Koch A, Hartmann A, Jorand R, Mottaghy DC, Pechnig R, Rath V, Wolf A. Erstellung statistisch abgesicherter thermischer und hydraulischer gesteinseigenschaften für den flachen und tiefen untergrund in deutschland: Phase 1 - westliche molasse und nördlich angrenzendes süddeutsches schichtstufenland; endbericht. Aachen: RWTH, 01.01.2005–31.10.2006; 2007.
Dalla Longa F, Nogueira LP, Limberger J, van Wees J-D, van der Zwaan B. Scenarios for geothermal energy deployment in Europe. Energy. 2020. https://doi.org/10.1016/j.energy.2020.118060.
Diersch H-J. FEFLOW-finite element modeling of flow, mass and heat transport in porous and fractured media. 1st ed. Berlin: Springer; 2014.
DWD. Annual mean temperatures of Germany; 2013. https://werdis.dwd.de.
Eyerer S, Schifflechner C, Hofbauer S, Bauer W, Wieland C, Spliethoff H. Combined heat and power from hydrothermal geothermal resources in Germany: an assessment of the potential. Renew Sustain Energy Rev. 2020. https://doi.org/10.1016/j.rser.2019.109661.
Fan Y, Zhang S, Huang Y, Pang Z, Li H. Determining the recoverable geothermal resources using a numerical thermo-hydraulic coupled modeling in geothermal reservoirs. Front Earth Sci. 2022. https://doi.org/10.3389/feart.2021.787133.
Franke W. The mid-European segment of the Variscides: tectonostratigraphic units, terrane boundaries and plate tectonic evolution. Geol Soc Lond Spec Publ. 2000;179:35–61. https://doi.org/10.1144/GSL.SP.2000.179.01.05.

Frey M, Weinert S, Bär K, Van Der Vaart J, Dezayes C, Calcagno P, Sass I. Integrated 3D geological modelling of the northern Upper Rhine Graben by joint inversion of gravimetry and magnetic data. Tectonophysics. 2021. https://doi.org/10.1016/j.tecto.2021.228927.
Freymark J, Sippel J, Scheck-Wenderoth M, Bär K, Stiller M, Kracht M, Fritsche J-G. Theterogeneous crystalline crust controls the shallow thermal field—a case study of Hessen (Germany). Energy Procedia. 2015;76:331–40. https://doi.org/10.1016/j.egypro.2015.07.837.
Freymark J, Sippel J, Scheck-Wenderoth M, Bär K, Stiller M, Fritsche J-G, Kracht M. The deep thermal field of the Upper Rhine Graben. Tectonophysics. 2017;694:114–29. https://doi.org/10.1016/j.tecto.2016.11.013.
Freymark J, Bott J, Cacace M, Ziegler M, Scheck-Wenderoth M. Influence of the main border faults on the 3D hydraulic field of the Central Upper Rhine Graben. Geofluids. 2019;2019:21. https://doi.org/10.1155/2019/7520714.
Garg SK, Combs J. A reformulation of USGS volumetric "heat in place" resource estimation method. Geothermics. 2015;55:150–8. https://doi.org/10.1016/j.geothermics.2015.02.004.
GeORG-Projektteam. Geopotenziale des tieferen untergrundes im oberrheingraben, fachlich-technischer abschlussbericht des interreg-projekts georg, teil 1: Ziele und ergebnisse des projekts. EU-Projekt GeORG; 2013a.
GeORG-Projektteam. Geopotenziale des tieferen untergrundes im oberrheingraben, fachlich-technischer abschlussbericht des interreg-projekts georg, teil 2: Geologische ergebnisse und nutzungsmöglichkeiten. EU-Projekt GeORG; 2013b.
GeORG-Projektteam. Geopotenziale des tieferen untergrundes im oberrheingraben, fachlich-technischer abschlussbericht des interreg-projekts georg, teil 3: Daten, methodik, darstellungsweise. EU-Projekt GeORG; 2013c.
GeORG-Projektteam. Geopotenziale des tieferen untergrundes im oberrheingraben, fachlich-technischer abschlussbericht des interreg-projekts georg, teil 4: Atlas. EU-Projekt GeORG; 2013d.
Gringarten AC. Reservoir lifetime and heat recovery factor in geothermal aquifers used for urban heating. Pure Appl Geophys. 1978;117:297–308. https://doi.org/10.1007/BF00879755.
Herrmann F. Entwicklung einer methodik zur großräumigen modellierung von grundwasserdruckflächen am beispiel der grundwasserleiter des bundeslandes hessen. PhD thesis, Brandenburgische Technische Universität Cottbus, Germany; 2010.
Hintze M, Plasse B, Bär K, Sass I. Preliminary studies for an integrated assessment of the hydrothermal potential of the Pechelbronn Group in the northern Upper Rhine Graben. Adv Geosci. 2018;45:251–8. https://doi.org/10.5194/adgeo-45-251-2018.
Hoth P, Seibt A, Kellner T. Chemische charakterisierung der thermalwässer. In: Geowissenschaftliche Bewertungsgrundlagen zur Nutzung Hydrogeothermaler Ressourcen in Norddeutschland. Potsdam: Geoforschungszentrum; 1997. p. 81–9.
Huang Y, Cheng Y, Ren L, Tian F, Pan S, Wang K, Wang J, Dong Y, Kong Y. Assessing the geothermal resource potential of an active oil field by integrating a 3D geological model with the hydro-thermal coupled simulation. Front Earth Sci. 2022. https://doi.org/10.3389/feart.2021.787057.
Jamieson DT, Tudhope JS, Morris GR. Cartwright physical properties of sea water solutions: heat capacity. Desalination. 1969;7:23–30. https://doi.org/10.1016/S0011-9164(00)80271-4.
Kastner O, Sippel J, Zimmermann G. Regional-scale assessment of hydrothermal heat plant capacities fed from deep sedimentary aquifers in Berlin/Germany. Geothermics. 2015;53:353–67. https://doi.org/10.1016/j.geothermics.2014.06.002.
Kivanc Ates H, Serpen U. Power plant selection for medium to high enthalpy geothermal resources of turkey. Energy. 2016;102:287–301. https://doi.org/10.1016/j.energy.2016.02.069.
Klügel T. Geometrie und kinematik einer variszischen plattengrenze-der suüdrand des rhenoherzynikums im taunus. Geologische Abhandlung Hessen. 1997;101:215.
Knoebel D, Chou JJ, Anderson R. Measurements of thermodynamic properties of saline solutions. Tech. rep., Oklahoma Water Resource Research Institute, Oklahoma State University, Stillwater, USA, OWRR Project Number A-009; 1968.
Koltzer N, Scheck-Wenderoth M, Bott J, Cacace M, Frick M, Sass I, Fritsche J-G. Bär: the effects of regional fluid flow on deep temperatures (Hesse, Germany). Energies. 2019. https://doi.org/10.3390/en12112081.
Lampe C, Person M. Advective cooling within sedimentary rift basins-application to the Upper Rhine Graben (Germany). Mar Pet Geol. 2002;19:361–75. https://doi.org/10.1016/S0264-8172(02)00022-3.
Limberger J, Boxem T, Pluymaekers M, Bruhn D, Manzella A, Calcagno P, Beekman F, Cloetingh S, van Wees J-D. Geothermal energy in deep aquifers: a global assessment of the resource base for direct heat utilization. Renew Sustain Energy Rev. 2018;82:961–75. https://doi.org/10.1016/j.rser.2017.09.084.
Lovekin J. Geothermal inventory. Bull Geotherm Resour Counc. 2004;33:242–4.
Ludwig F. Geogene hintergrundwerte der hauptbestandteile und spurenstoffe in hessischen grundwässern. Geologische Abhandlungen Hessen. 2013;118:1–165.
Lund JW. Utilization of geothermal resources. Klamath Falls: Geo-Heat Center, Oregon Institute of Technology; 2018.
Magri F, Akar T, Gemici U, Pekdeger A. The feasibility and potential of geothermal heat in the deep Alberta foreland basin-Canada for CO_2 savings. Renew Energy. 2014;66:541–9. https://doi.org/10.1016/j.renene.2013.12.044.
Marrero-Diaz R, Ramalho E, Costa A, Ribeiro L, Carvalho J, Pinto C, Rosa D, Correia A. Updated geothermal assessment of Lower Cretaceous aquifer in Lisbon region, Portugal. In: Proceedings world geothermal congress, Melbourne, Australia; 2015.
Muffler P, Cataldi R. Methods for regional assessment of geothermal resources. Geothermics. 1978;7:53–89.
Nathenson M. Physical factors determining the fraction of stored energy recoverable from hydrothermal convection systems and conduction-dominated areas. U.S. Geol. survey open-file report; 1975. p. 75–525.
Nayar KG, Sharqawy MH, Banchik LD, Lienhard V JH. Thermophysical properties of seawater: a review and new correlations that include pressure dependence. Desalination. 2016;390:1–24.
NOAA National Geophysical Data Center. Etopo1 1 arc-minute global relief model. Washington, DC: NOAA National Centers for Environmental Information; 2009. https://doi.org/10.7289/V5C8276M.
Noack V, Scheck-Wenderoth M, Cacace M. Sensitivity of 3D thermal models to the choice of boundary conditions and thermal properties: a case study for the area of Brandenburg (NE German basin). Environ Earth Sci. 2012;67:1695–711. https://doi.org/10.1007/s12665-012-1614-2.

O'Sullivan M, O'Sullivan J. Reservoir modeling and simulation for geothermal resource characterization and evaluation. In: Geothermal power generation. Duxford: Woodhead Publishing; 2016. p. 165–99. https://doi.org/10.1016/B978-0-08-100337-4.00007-3.
Paradigm Holding LLC. Paradigm: user guide part IV foundation modeling. Nashville: Paradigm Holding LLC; 2009.
Paschen H, Oertel D, Grünwald R. Möglichkeiten geothermischer stromerzeugung in deutschland. Sachstandsbericht. Technical report, Büro für Technikfolgen-Abschätzung beim Deutschen Bundestag (TAB); 2003. https://doi.org/10.5445/IR/1000103222.
Pribnow D, Clauser C. Heat and fluid flow at the soultz hot dry rock system in the Rhine Graben. In: Proceedings world geothermal congress, Kyushu-Tohoku, Japan; 2000. http://www.geothermal-energy.org/pdf/IGAstandard/WGC/2000/R0467.PDF.
Rogge S, Kaltschmitt M. Electricity and heat provision from geothermal energy. An economic analysis; strom- und waermebereitstellung aus erdwaerme. Eine oekonomische analyse. Erdoel Erdgas Kohle; 2002.
Rühaak W, Bär K, Sass I. Combining numerical modeling with geostatistical interpolation for an improved reservoir exploration. Energy Procedia. 2014;59:315–22. https://doi.org/10.1016/j.egypro.2014.10.383.
Rybach L. "The future of geothermal energy" and its challenges. In: Proceedings world geothermal congress, Bali, Indonesia; 2010.
Sanyal S, Butler SJ. An analysis of power generation prospects from enhanced geothermal systems. Trans Geotherm Resour Counc. 2005;29:131–8.
Sass I, Weinert S, Bär K. Success rates of petroleum and geothermal wells and their impact on the European geothermal industry. Swiss Bulletin für angewandte Geologie. 2017;21:57–65. https://doi.org/10.5169/seals-658197.
Schäffer R, Bär K, Fischer S, Fritsche J-G, Sass I. Database of mineral, thermal and deep groundwaters of Hesse, Germany; 2020.
Schäffer R, Bär K, Fischer S, Fritsche J-G, Sass I. Mineral, thermal and deep groundwater of Hesse, Germany. Earth System Sci Data. 2021;13:4847–60. https://doi.org/10.5194/essd-13-4847-2021.
Scheck-Wenderoth M, Frick M, Cacace M, Sippel J. Overcoming spatial scales in geothermal modeling for urban areas. Energy Procedia. 2017;125:98–105. https://doi.org/10.1016/j.egypro.2017.08.080.
Schellschmidt R, Sanner B, Pester S, Schulz R. Geothermal energy use in Germany. In: Proceedings world geothermal congress 2010, Bali, Indonesia; 2010.
Sharqawy MH, Lienhard JH, Zubair SM. Thermophysical properties of seawater: a review of existing correlations and data. Desalin Water Treat. 2010;16:354–80. https://doi.org/10.5004/dwt.2010.1079.
Squillacote AH, Ahrens J, Law C, Geveci B, Moreland K, King B. The paraview guide. New York: Kitware Clifton Park; 2007.
Stein E. The geology of the Odenwald crystalline complex. Mineral Petrol. 2001;72:7–28. https://doi.org/10.1007/s007100170024.
Stober I, Bucher K. Hydraulic and hydrochemical properties of deep sedimentary reservoirs of the Upper Rhine Graben, Europe. Geofluids. 2015;15:464–82. https://doi.org/10.1111/gfl.12122.
Trumpy E, Botteghi S, Caiozzi F, Donato A, Gola G, Montanari D, Pluymaekers MPD, Santilano A, van Wees JD, Manzella A. Geothermal potential assessment for a low carbon strategy: a new systematic approach applied in southern Italy. Energy. 2016;103:167–81. https://doi.org/10.1016/j.energy.2016.02.144.
Van Der Vaart J, Bär K, Frey M, Reinecker J, Sass I. Quantifying model uncertainty of a geothermal 3D model of the Cenozoic deposits in the northern Upper Rhine Graben, Germany. Zeitschrift der Deutschen Gesellschaft für Geowissenschaften. 2021;172:365–79. https://doi.org/10.1127/zdgg/2021/0286.
van Wees J-D, Kronimus A, van Putten M, Pluymaekers MPD, Mijnlieff H, van Hooff P, Obdam A, Kramers L. Geothermal aquifer performance assessment for direct heat production—methodology and application to Rotliegend aquifers. Neth J Geosci. 2012;91–4:651–65. https://doi.org/10.1017/S0016774600000433.
Vogel B. Untersuchung und modellierung der mitteltiefen geothermischen potenziale des buntsandsteins in nordosthessen. Unpublished Master Thesis, TU Darmstadt; 2020.
Vosteen H-D, Schellschmidt R. Influence of temperature on thermal conductivity, thermal capacity and thermal diffusivity for different types of rock. Phys Chem Earth. 2003;28:499–509. https://doi.org/10.1016/S1474-7065(03)00069-X.
Wang Y, deHoop S, Voskov D, Bruhn D, Bertotti G. Modeling of multiphase mass and heat transfer in fractured high-enthalpy geothermal systems with advanced discrete fracture methodology. Adv Water Resour. 2021;154: 103985. https://doi.org/10.1016/j.advwatres.2021.103985.
Weinert S, Bär K, Sass I. Database of petrophysical properties of the mid-German crystalline rise. Earth Syst Sci Data. 2021;13:1441–59. https://doi.org/10.5194/essd-13-1441-2021.
Williams CF. Updated methods for estimating recovery factors for geothermal resources. In: Proceedings, 32th workshop on geothermal reservoir engineering, Stanford University; 2007.
Williams CF. Thermal energy recovery from enhanced geothermal systems—evaluating the potential from deep, high-temperature resources. In: Proceedings, 35th workshop on geothermal reservoir engineering, Stanford University; 2010.
Williams C, Reed M, Mariner R. A review of methods applied by the us geological survey in the assessment of identified geothermal resources. Open-file report 2008-1296, U.S. Geological Survey; 2008.
Zarrouk SJ, Moon H. Efficiency of geothermal power plants: a worldwide review. Geothermics. 2014;51:142–53. https://doi.org/10.1016/j.geothermics.2013.11.001.

Publisher's Note